IEEE TRANSACTIONS ON ANTENNAS AND PROPAGATION, Citation information: DOI 10.1109/TAP.2020.3030942.

Transmit-Receive Parabolic Reflectarray to Generate Two Beams per Feed for Multi-Spot Satellite Antennas in Ka-Band

Daniel Martinez-de-Rioja, *Student Member, IEEE*, Eduardo Martinez-de-Rioja, *Member, IEEE,* Yolanda Rodriguez-Vaqueiro*, Member, IEEE,* Jose A. Encinar, *Fellow, IEEE*, Antonio Pino, *Senior Member, IEEE*, Marcos Arias, and Giovanni Toso, *Senior Member, IEEE*

***Abstract*—This contribution describes the design of a multibeam parabolic reflectarray to produce two adjacent beams per feed in orthogonal Circular Polarization (CP) simultaneously at transmit (Tx) and receive (Rx) frequencies in Ka-band. The Variable Rotation Technique (VRT) has been applied to reflectarray cells based on two types of resonant elements, which makes it possible to provide orthogonal beams at Tx and Rx, as well as to implement an in-band optimization procedure to reduce the cross-polarization. A 90-cm parabolic reflectarray has been designed, manufactured and tested to produce multiple adjacent beams in RHCP and LHCP at both 20 and 30 GHz. The results are satisfactory and validate the concept of generating two spaced beams in orthogonal CP by a single feed, changing the polarization of the beam between Tx and Rx. This concept can be suitable for multispot satellites in Ka-band, enabling to halve the number of onboard antennas and feeds.**

***Index Terms*—Reflectarray, multibeam antennas, dual band, circular polarization, satellite antennas, Ka-band.**

I. Introduction

HIGH throughput satellites (HTS) in Ka-band split the service area into a cellular coverage made up of a high number of spots [1]. For both transmission (Tx) and reception (Rx) bands, the beams are generated at two different frequency sub-bands (f_1, f_2) and in two orthogonal polarizations (p_1, p_2), giving rise to a four-color reuse scheme [2], as shown in Fig. 1. Typically, four reflectors are required onboard the satellite, operating by a Single-Feed-Per-Beam configuration (each reflector produces the beams associated to a single color at Tx and Rx). Several antenna solutions have been proposed to reduce the number of onboard antennas [3]-[5], but the cost in efficiency, stowage capacity or complexity is too high compared to the current architecture. Reflectarrays have also been proposed due to their independent operation at different frequencies or polarizations [6].

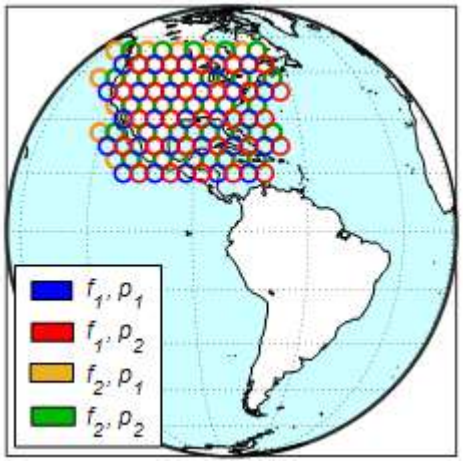

Fig. 1 Multispot coverage in a four-color reuse scheme.

Reflectarrays can easily operate in dual linear polarization (LP) [7], [8]; however, satellite communications in Ka-band operate in dual circular polarization (CP). The design of reflectarrays to operate independently in dual-CP has widely been studied in the last years: different solutions have been proposed based on polarization selective layers or polarizer layers [9]-[11]. Other solutions are focused on the Variable Rotation Technique (VRT), which makes it possible to introduce opposite phase-shifts in orthogonal CP's [12]-[13]. A parabolic reflectarray was proposed in [14], where the

This work has been supported in part by the Spanish Ministry of Economy and Competitiveness under the project TEC2016-75103-C2-1-R, and under the project FJCI-2016-29943; by the European Regional Development Fund (ERDF), and by the European Space Agency (ESA) under contract 4000117113/16/NL/AF.

D. Martinez-de-Rioja and J. A. Encinar are with the Information Processing and Telecommunications Center, Universidad Politécnica de Madrid (UPM), 28040 Madrid, Spain (e-mail: {jd.martinezderioja, jose.encinar}@upm.es).

E. Martinez-de-Rioja is with the Dept. of Signal Theory and Communications, Universidad Rey Juan Carlos, 28942 Madrid, Spain (e-mail: eduardo.martinez@urjc.es).

A. Pino, Y. Rodriguez-Vaqueiro and M. Arias are with the Signal Theory and Communications Dept., Universidade de Vigo, 36310 Vigo, Spain (e-mail: {agpino, yrvaqueiro, marcos}@com.uvigo.es).

G. Toso is with the Antenna and Sub-Millimeter Wave Section, Electromagnetics Division, European Space Agency ESTEC, 2200 AG Noordwijk, The Netherlands (e-mail: giovanni.toso@esa.int).

parabolic surface focuses the reflected field while the VRT is used to deviate in opposite directions the beams in each orthogonal CP. This concept has been validated experimentally in [15] for a flat reflectarray. In [16] a flat reflectarray deviates the beams in orthogonal CP by VRT at the same time that introduces phase corrections to shape the beams without the need for a parabolic surface.

The antennas described in [14]-[16] operate in a single frequency band. In [17], a reflectarray cell has been proposed to operate by VRT at both Tx and Rx frequencies in Ka-band. A flat reflectarray prototype has recently validated the dual-band, dual-CP operation in [18] using the cell described in [17]. Moreover, a 0.65-m parabolic reflectarray with the same operating principle has been proposed in [19] and recently validated in [20] to generate two beams per feed in dual CP at Tx and Rx in Ka-band. In [20], a dual-band reflectarray cell with a split hexagonal-loop around a rectangular patch was used to independently adjust the phases at Tx and Rx frequencies, respectively. The cell from [20] presents less degrees of freedom to adjust the phases at Rx than the cell shown in [17], where two orthogonal sets of three parallel dipoles are used instead of the rectangular patch from [20].

A critical limitation of the previous tested reflectarrays to operate by VRT is the reduction of the cross-polar discrimination (XPD) within the operating frequency bands: in [15], [16] the XPD reaches a minimum value around 10 dB. In [20], the results of XPD are only provided at central frequencies, and it is said that both XPD and C/I deteriorates outside the design frequencies, suggesting that a further optimization must be carried out in a future work to overcome these limitations. In this paper, the degrees of freedom provided by the cell presented in [17] are used to implement an optimization technique within the operational bandwidth [18] to improve the XPD, as suggested in [20]. A 0.9 m parabolic multilayer reflectarray antenna has been designed, manufactured and tested for the first time, with the purpose of generating two spaced beams per feed in dual CP with improved XPD in a 500-MHz bandwidth for Tx and Rx in Ka-band. There are two main improvements with respect to the work presented in [20]:

1) The generation of orthogonal beams at Tx and Rx, which is a usual requirement for multispot coverages in Ka-band that increases the difficulty of the dual-band design by VRT.

2) The implementation of an in-band optimization to reduce the cross-polar radiation and the maximum directivity at Rx to match the beam shaping at Tx and Rx, which is possible by the additional degrees of freedom provided by the three parallel dipoles for each polarization in the proposed cell [17].

These improvements are achieved at the cost of manufacturing a dual-layer reflectarray, with a small increase of the complexity in terms of computational burden and manufacturing with respect to a single-layer reflectarray [20].

In addition to the parabolic reflectarray, a reflector has been fabricated using the same manufacturing process. The measured performance of both antennas has been compared.

II. Mission Scenario

This contribution proposes the use of a parabolic reflectarray to generate two spaced beams in orthogonal CP per feed simultaneously at Tx and Rx frequencies, with application in HTS systems, since a multi-fed offset parabolic reflectarray could generate half the beams of a four-color multispot coverage. A 1.8 m parabolic reflectarray should be required to fulfil the specifications in gain defined in HTS systems. Due to the large size of the satellite antenna, the parabolic reflectarray prototype has been scaled by a factor of two (a diameter of 0.9 m). The main parameters of a complete antenna system, according to the requirements commonly specified in real HTS applications [21], are defined in Table I together with the adapted requirements to the scaled prototype.

TABLE I
Antenna System Requirements

Parameter	System	Scaled prototype
Number of spots	> 100	2 spots/feed
Spot lattice	Triangular	Triangular
Spot diameter	0.65º	1.3º
Spot separation	0.56º	1.18º
EOC gain	> 43.8 dBi	> 39 dBi
Roll-off factor	< 4.3 dB	< 4.3 dB
Single Entry C/I	> 20 dB	> 20 dB
Co-polar / cross-polar	> 20 dB	> 20 dB
Tx frequencies	19.2 GHz - 20.2 GHz	19.45 GHz - 19.95 GHz
Rx frequencies	29.0 GHz - 30.0 GHz	29.25 GHz - 29.75 GHz

The Edge Of Coverage (EOC) gain is defined as the gain level where the spot diameter matches the required value (1.3º for the proposed prototype). Since only one antenna has been designed, it was decided to maintain the central Tx and Rx frequencies (19.7 and 29.5 GHz) for the prototype, with 500-MHz bands. The co-polar over cross-polar ratio is computed as the XPD at Tx and the cross-polar isolation (XPI) at Rx.

III. Antenna Definition

A. Definition of the Reflectarray Cell

The reflectarray cell is a two-layer configuration with two outer symmetrical circular arcs to operate at Tx, and two orthogonal stacked sets of three coupled parallel dipoles to operate at Rx, as shown in Fig. 2. The cell has been defined and characterized in [17], including the experimental validation of a home-made electromagnetic code based on the SD-MoM [22], [23], used for the efficient analysis of the cell response under any angle of incidence. Recently, the same cell has been used in a flat reflectarray prototype [18]. The cell is able to provide an opposite phase shift in each CP at both Tx and Rx frequencies by the independent rotation of the arcs and dipoles, and the adjustment of their lengths: l_{A1}, l_{A2}, l_{B1} and l_{B2} for the dipoles, and the angle Ω for the arc (see Fig. 2).

Two 0.787 mm sheets of IsoClad 933 (nominal values: ε_r = 2.33, tanδ = 0.0016) have been used for both dielectric layers of the cell. IsoClad 933 provides the necessary flexibility to use on double-curved surfaces with high dimensional stability and mechanical strength [24]. Materials previously used in space applications should be considered for a real scenario,

such as Qzll/EX-1516, based on a prepreg fabric with quartz fibers and low loss resin, with a germanium coating on the reflectarray elements printed on Kapton to avoid electrostatic discharges (ESD) because of the small conductivity of the germanium coating [25]. The arcs and the upper dipoles will be printed on the top side of the upper Isoclad sheet, while the lower dipoles will be printed on the bottom side of the same sheet. Two layers of 38 μm CuClad 6250 bolding film (ε_r = 2.32, tanδ = 0.0013) have been used to bond the two Isoclad sheets. The widths of the arcs and dipoles are 0.2 and 0.4 mm, respectively, the inner radius of the arcs is 2.65 mm, and the separation between dipoles is 1.2 mm from center to center.

The way to obtain the final cell distribution on the parabolic surface consists on computing a grid of reflectarray cells with constant dimensions along both *x* and *y*-axis (P_X and P_Y, respectively) placed in the aperture plane of the paraboloid (the area enclosed by the rim of the dish). In this case, the initial dimensions have been fixed to P_X = 6.3 mm and P_Y = 6.5 mm, since the incidence angles on the reflectarray will be larger along the *x*-axis than along the *y*-axis. Then, the periodic grid is projected over the parabolic surface, resulting in a grid of reflectarray cells with slightly variable sizes. Due to the low curvature of the antenna, each cell is analyzed by SD-MoM considering a locally flat and periodic structure, but using the real values of period, angle of incidence and field components corresponding to the position of the cell in the antenna, without any interpolation or look-up table.

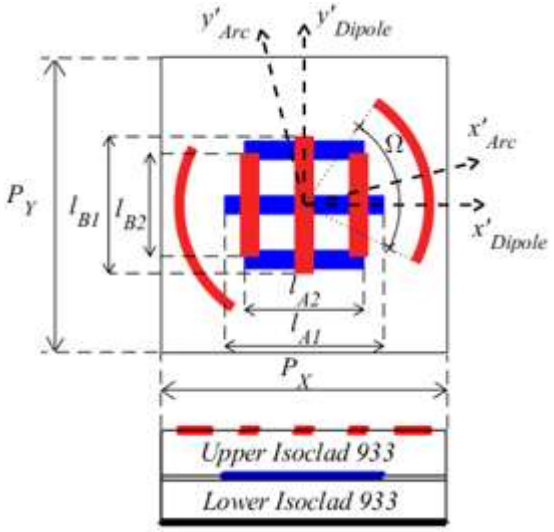

Fig. 2 Top view and lateral view of the reflectarray cell

B. Prototype Configuration

Based on the antenna configuration that would be required in a real HTS, a prototype has been defined whose dimensions are scaled by a factor of two. The demonstrator consists of a 0.9 m parabolic reflectarray formed by 15,748 cells. The geometric parameters of the antenna are shown in Table II.

The reflectarray was conceived to be illuminated by a cluster of seven feeds to generate fourteen beams, as shown in Fig. 3 in the normalized angular coordinates u = sinθ·cosφ, v = sinθ·sinφ, where the position of the central horn matches the focus of the paraboloid. However, since the antenna system is symmetric with respect to the *xz* plane (see Fig. 4) and to simplify the mechanical design, the manufactured prototype considers three different positions of the feed: feed 1, 2 and 3 in Fig. 3, generating six beams. A 60-mm diameter dual-band feed-horn developed by Anteral [26] has been used to illuminate the demonstrator. The horn has a directivity of around 21.5 dBi at 19.7 GHz and 23.5 dBi at 29.5 GHz, with a minimum XPD of around 25 dB at both bands. The field radiated by the horn has been modeled using a spherical wave expansion (SWE) distribution. The phase center of the feed at Rx is shifted with respect to Tx, producing a reduction in gain of around 0.5 dB at Rx (this effect is included in the SWE distribution). A half-subtended angle of 18º has been estimated to get an edge illumination level of -12 dB at 19.7 GHz and -18 dB at 29.5 GHz. The feed chain also includes a commercial polarizer for terminal stations (ground segment) from General Dynamics [27] with an operational band from 19.4 to 21.20 GHz for Tx, and from 29.2 to 31 GHz for Rx (model 0183-1416). The polarizer has nominal insertion losses lower than 0.45 dB at Tx and 0.35 dB at Rx, with an axial ratio (AR) lower than 2.3 dB at Tx and 1.5 dB at Rx. The effect of the polarizer is not considered in the simulations. The 3D CAD model of the antenna prototype can be seen in Fig. 4.

TABLE II
GEOMETRY OF THE PARABOLIC REFLECTARRAY DEMONSTRATOR

Parameter	Requirement
Aperture diameter (D)	906 mm
Focal length (f)	1359 mm
Offset height (h_0)	628 mm
Clearance	175 mm
Half subtended angle	18 º

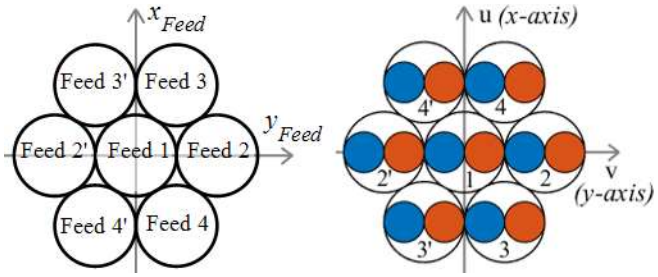

Fig. 3 Feed array and its associated spot distribution for the reflectarray.

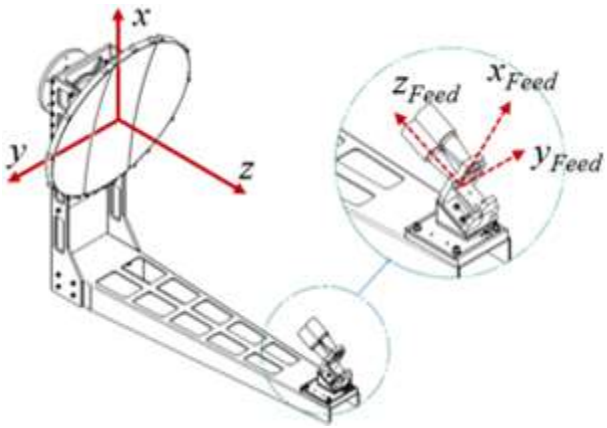

Fig. 4 3D CAD model of the complete antenna breadboard and detailed view of the assembly implemented to change the position of the feed.

IV. Antenna Design and Simulated Results

A. Design process of the Antenna

The rotation angle and dimensions of each group of reflectarray elements are obtained after a step-by-step design process that takes into account the requirements imposed by the VRT and the phase shift distributions required on the reflectarray. The electromagnetic analysis of the reflectarray antenna has been performed by means of a combination of Physical Optics (PO) technique [28] with a realistic model of the reflectarray surface reflection, characterized by SD-MoM considering an infinite periodic surface [22], [23].

The VRT makes it possible to introduce opposite phase-shifts between the orthogonal CP components of the reflected field, where the phase delay introduced in each CP is proportional to twice the rotation angle of the elements [12]. As proposed in [14], the VRT is used to deviate the beams, while the parabolic surface of the antenna focuses the beams. The rotation angles of the arcs and dipoles are fixed as the phase distributions at Tx and Rx, respectively, divided by two. Every beam at Tx is generated in the orthogonal CP than the beam at Rx (see Fig. 5), following a real requirement of satellite antenna farms. This operation means that the arcs and dipoles rotate in opposite senses, which generates larger differences between the geometry of adjacent cells that increase the difficulty of the antenna design (in [20] the elements rotate in the same sense, generating Tx and Rx beams with the same CP). The VRT requires to ensure a 180º phase difference between the two orthogonal linear components of the reflected field to suppress the cross-polar component [12]. Thus, the length of the rotated elements must be adjusted to fulfil this requirement at Tx and Rx [17].

The aforementioned phase distributions only deviate the beams, producing narrower beams at Rx, due to the larger electrical size of the antenna. As described in [17], the dipoles can be adjusted to control the absolute phase values in the linear components of the field where the 180º phase difference must be fulfilled, making it possible to introduce phase corrections to slightly reduce the directivity at Rx to accomplish the roll-off requirement given in Table I. The difference between introducing or not the phase corrections at 29.5 GHz can be seen in Fig. 5, which shows the simulated cuts of the radiation pattern for the designed parabolic reflectarray at 29.5 GHz including both cases, and also the cuts at 19.7 GHz. The simulated response at Tx is barely influenced by the phase correction at Rx, while the Rx response presents a reduction of 0.6 dB in the maximum gain as well as a reduction in the side lobe level (SLL). The cuts of the radiation patterns include masks to check the compliance with the requirements. The masks consist of a minimum gain level of 40 dBi with a beamwidth of 1.3º in the coverage zone of the beam, together with a maximum SLL that is 20 dB below the previous level and is centered in the coverage area of the adjacent beams (left and right) in the same color.

Previous reflectarrays that operate by VRT [15], [16], [20] present low levels of XPD, mostly attributed to a narrow band performance of the reflectarray cells to provide the 180º phase difference between the orthogonal linear components of the reflected field. As stated in [18], the arcs at Tx present a more stable behavior in band than the dipoles at Rx. Thus, an optimization has been included to reduce the cross-polar radiation in the Rx band. The in-band optimization procedure, described in [18], tries to minimize an error function related to the aforementioned phase difference at the extreme and central Rx frequencies (ideally 180º), and it is implemented cell by cell through an adjustment of the dipoles lengths accounting for the real periods, angles of incidence, and field components on each cell, without any interpolation or look-up table.

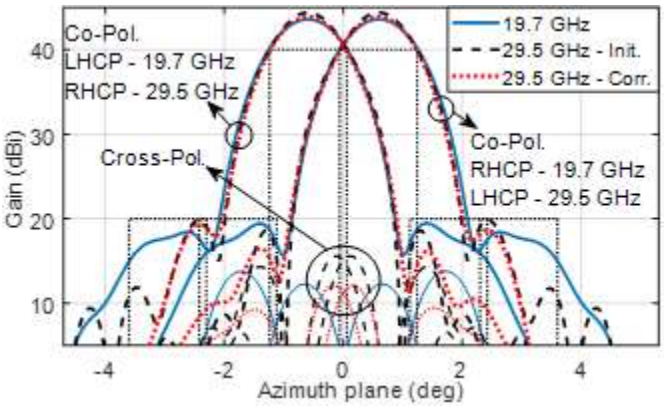

Fig. 5 Simulated radiation patterns for the demonstrator illuminated by a dual-CP feed placed at the focal point of the paraboloid.

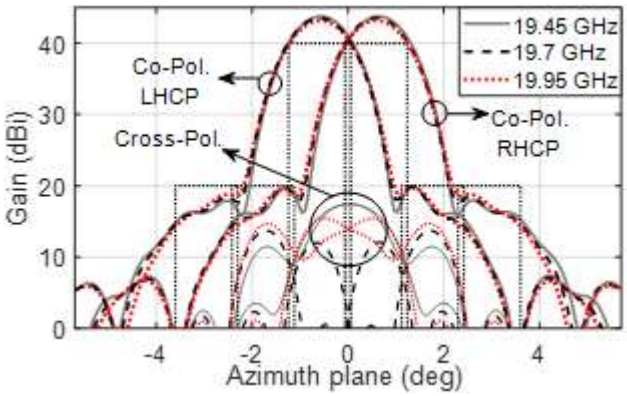

Fig. 6 Simulated radiation patterns for the demonstrator illuminated by a dual-CP feed at the extreme and central frequencies of the Tx band.

The azimuth plane of the simulated radiation patterns at the extreme and central frequencies of each band for the designed parabolic reflectarray is shown in Fig. 6 and Fig. 7 when the reflectarray is illuminated by a dual-CP feed placed at the focal point of the paraboloid. The radiation patterns at Tx show a XPD larger than 20 dB that meet the requirements shown in Table I. Fig. 7 includes the radiation patterns at Rx before (Fig. 7(a)) and after (Fig. 7(b)) implementing the in-band optimization. In Fig. 7(a), the minimum of cross-polar radiation is achieved at the design frequency, 29.5 GHz (where the XPI is around 25 dB); however, at the extreme frequencies the XPI is reduced to 13 dB. The radiation patterns of the in-band optimized design shown in Fig. 7 (b) achieve an XPI larger than 20 dB for the complete band.

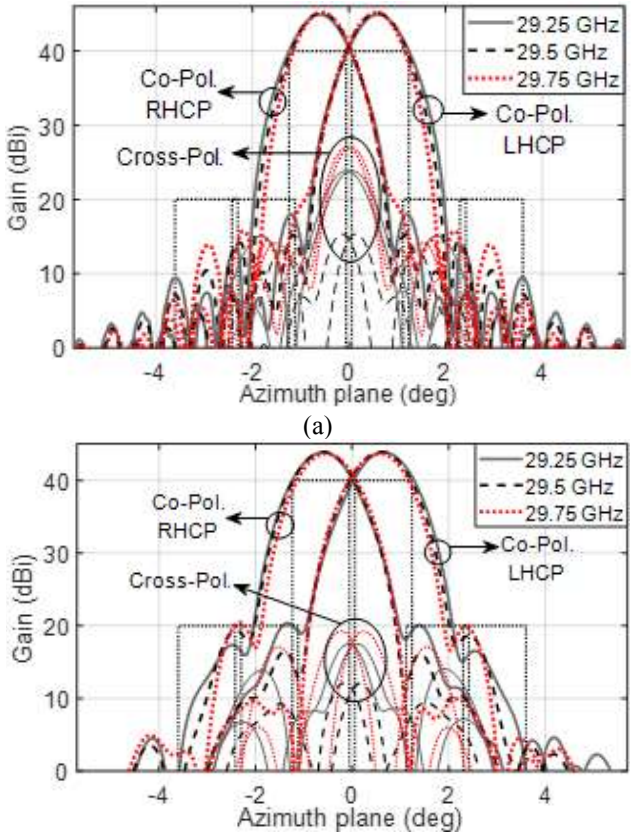

Fig. 7 Simulated radiation patterns for the demonstrator illuminated by a dual-CP feed at the extreme and central frequencies of the Rx band for (a) a non-optimized design and (b) an in-band optimized design.

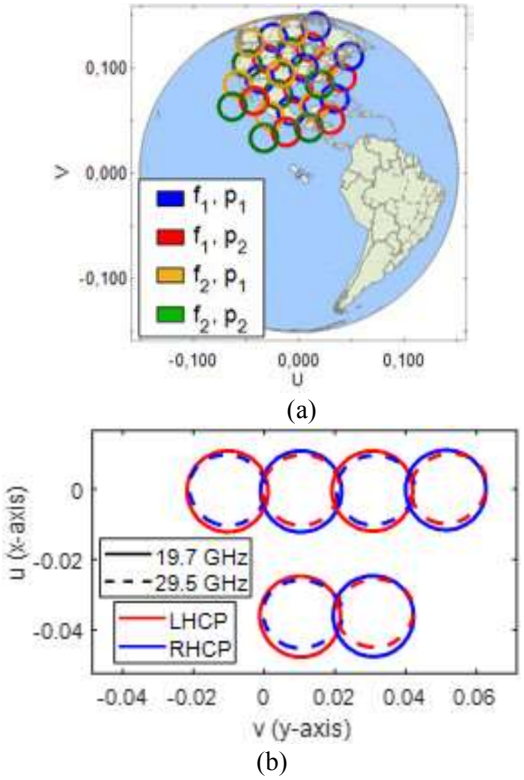

Fig. 8 (a) 28 spots generated by two 0.9 m reflectarrays with 7 feeds. (b) Contours of 6 beams generated by one reflectarray at 19.7 GHz and 29.5 GHz.

B. *Simulated Multibeam Performance*

The radiation patterns of the beams corresponding to the three horns (Feed 1, 2 and 3 in Fig. 3) have been computed at both Tx and Rx bands. Fig. 8 shows the coverage that would be obtained by two reflectarrays illuminated by the feed array shown in Fig. 3 considering an antenna boresight rotation angle of 75º, together with the simulated pattern contours of the 6 spot-beams at the same gain level (40 dBi) generated by feeds 1, 2 and 3 in dual CP at 19.7 GHz and 29.5 GHz. As required, the Tx and Rx beams are produced in orthogonal CP.

The simulated beams have been evaluated by means of the cuts of the radiation patterns parallel to the principal planes of the triangular spot grid. The cuts in 'u = 0' are presented in Fig. 9 and Fig. 10 at 19.7 and 29.5 GHz. The beams at 19.7 GHz show a maximum gain of 43.5 dBi with an EOC gain of 40.1 dBi. The single-entry C/I and XPD are larger than 19.5 dB and 29 dB, respectively. The simulations at 29.5 GHz present a maximum gain of 43.8 dBi, an EOC gain of 39.5 dBi, a minimum single-entry C/I and XPI of 18.3 dB and 25.5 dB, respectively. The minimum values of C/I are produced by the beams placed out of the focal point of the paraboloid, which are slightly degraded. The estimated values of the aggregated C/I are better than 14 dB at both Tx and Rx bands.

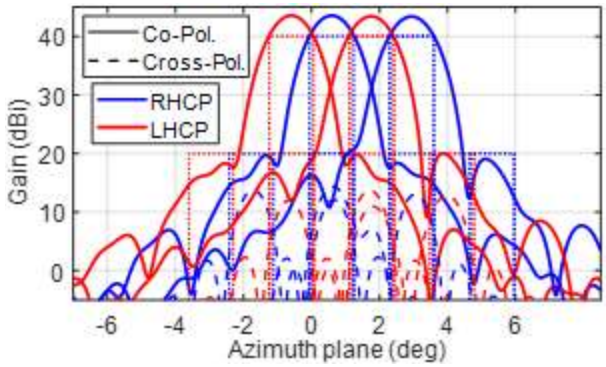

Fig. 9 Simulated radiation patterns for the beams generated by feeds 1 and 2 for the cut 'u = 0' in LHCP and RHCP at 19.7 GHz.

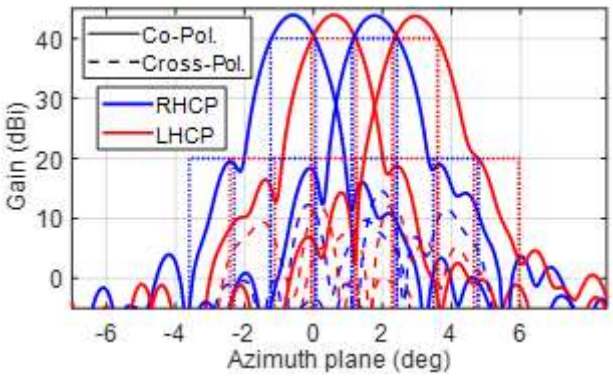

Fig. 10 Simulated radiation patterns for the beams generated by feeds 1 and 2 for the cut 'u = 0' in LHCP and RHCP at 29.5GHz

The previous simulations have considered only the central frequencies of the Tx and Rx bands. As shown in Fig. 6 and Fig. 7, the limitation in bandwidth imposed by the cross-polarization has been overcome by the implementation of an in-band optimization, which makes it possible to meet the

cross-polar requirements within 500 MHz bands.

V. Manufacturing Process of the 0.9 Meter Parabolic Reflectarray and a Reference Reflector Antenna

The manufacturing of the copper impressions by photo-etching on the IsoClad 933 material was undertaken by the company Trackwise [29]. Due to the large size of the antenna, the upper dielectric layer of the reflectarray, with printed elements on both internal and external sides, was divided in three bands (each around 30-cm wide), as can be seen in the CAD drawing of Fig. 4. The second layer, which has not any copper pattern on one side and it is covered by copper on the bottom surface (ground plane), was divided in two bands oriented perpendicular to the three bands of the previous layer.

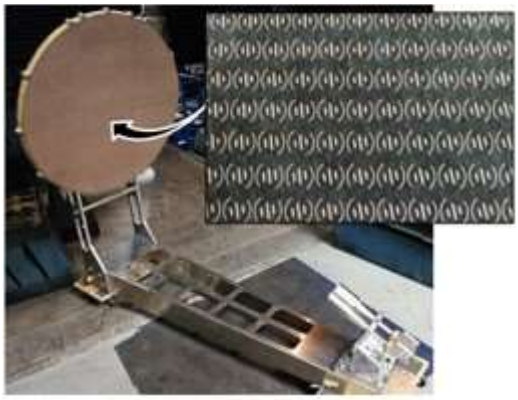

Fig. 11 Manufactured 0.9 m parabolic reflectarray demonstrator.

Then, the manufacturing process of the antenna system was developed by Acom Sistemas [30]. It includes the manufacture of the Carbon Fiber Reinforced Polymer (CFRP) parabolic sandwich, its integration with the printed arrays on Isoclad 933, and an aluminum support structure to install the feed chain in three different positions (see the CAD model in Fig. 4). First, a low-cost CFRP parabolic mold was manufactured. Then, the three bands with the printed arrays on both sides of the Isoclad 933 were adapted to the mold, as well as the second layer of the Isoclad 933 material cladded with copper on the bottom face, bonded together with the thermoplastic bonding film Cuclad 6250. The final parabolic reflectarray before entering the anechoic chamber of the Universidad Politécnica de Madrid (UPM) can be seen in Fig. 11. A 3D dimensional test of the mold has showed that the Root-Mean-Square (RMS) deviation with respect to the nominal parabolic surface was 0.042 mm. To improve the surface accuracy, an aluminum or Invar mold can be used. In addition, to ensure the necessary thermal stability for space missions, a suitable thermomechanical design of the structural sandwich should be accomplished. Note that the impact of thermo-elastic distortions should be smaller than in conventional "shaped" reflectors despite the presence of dielectrics, because the beam deviation at both bands and the shaping at Rx is produced by the rotated printed elements and not by the shaping of the reflector surface. The manufacturing process is directly compatible with those used for space CFRP reflectors and dichroic subreflectors used in scientific space missions [31].

Moreover, a reference parabolic reflector with the same configuration than the parabolic reflectarray has also been manufactured and measured in order to compare the performance of the reflectarray with a conventional reflector of identical geometry, and also to identify possible sources of error related to the feed system, antenna alignment, or the antenna structure. The reflector surface has been manufactured by using the same CFRP mold as the reflectarray, changing the dielectric sheets by a copper laminate also divided in three identical bands as the reflectarray prototype.

VI. RF Test of the Reflectarray Breadboard

A. Measurements of the Parabolic Reflectarray

The manufactured reflectarray and reflector have been measured at the Tx frequencies of 19.2, 19.45, 19.575, 19.7, 19.825, 19.95, and 20.2 GHz, and at the Rx frequencies of 29, 29.25, 29.375, 29.5, 29.625, 29.75, 30, 30.25 and 30.5 GHz (the last two frequencies have been tested only for the reflectarray). The measurements have been carried out at the anechoic chamber of the UPM, in a planar near-field measurement system (see Fig. 12), within an angular range of $-0.275 < u < 0.275$, $-0.275 < v < 0.275$. The measurements shown in this section represent directivity levels, since the measurement system provides a larger uncertainty in gain (± 0.5 dB) than in directivity (± 0.2 dB).

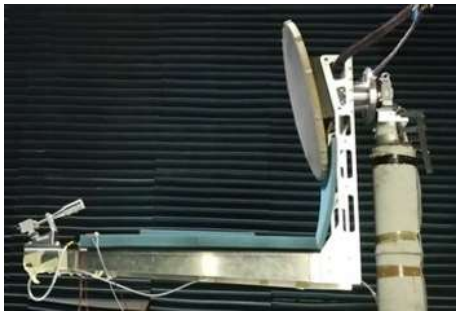

Fig. 12 Manufactured 0.9 m parabolic reflectarray in the planar near-field measurement system of the UPM.

The measurements of the parabolic reflectarray have been carried out for each position of the feed (central, lateral and upper position) considering both CP and both frequency bands. Fig. 13 shows the measured multi-spot coverage provided by the parabolic reflectarray at 19.7 GHz and 29.5 GHz. The measured beams generated by the reflectarray at 19.7 GHz reach values of maximum directivity close to 44 dBi, while the beams generated at 29.5 GHz present a maximum directivity around 45 dBi. In contrast, the reflector provides a measured maximum directivity of 44.1 dBi and 45.8 dBi at 19.7 GHz and 29.5 GHz, respectively. As expected, the reflectarray at 29.5 GHz provides a smaller directivity than the reflector since the printed dipoles are optimized to reduce the directivity at the Rx band.

Fig. 14 shows the 40.6 dBi-pattern contours of the measured spot-beams generated at 19.7 and 30 GHz by the reflectarray together with the 39.6 dBi-pattern contours of the measured beams at 30 GHz generated by the reference

reflector. Since the reflector cannot discriminate between CP, it generates 3 spot-beams, one per each feed position. The level of the contours has been selected to provide the required spot diameter (1.3º). Note that the reflectarray provides the same EOC gain at both Tx and Rx bands, while the reference reflector provides an EOC gain of 39.6 dBi at 30 GHz, exceeding the maximum required value of the roll-off factor (the reflector provides the same EOC gain at Tx as the reflectarray). Fig. 15 shows the contours of the measured beams produced by the reflectarray at 40.6 dBi (EOC gain), and 20.6 dBi (20 dB below the EOC gain), to appreciate the possible interferences between spots in the same color.

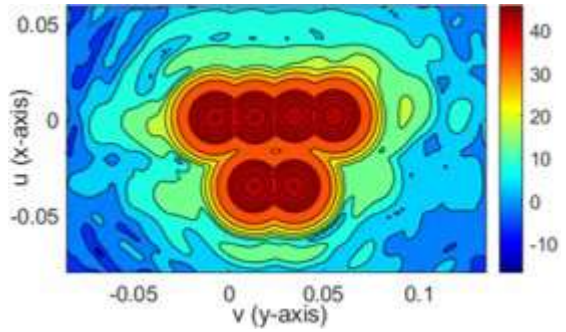

(a)

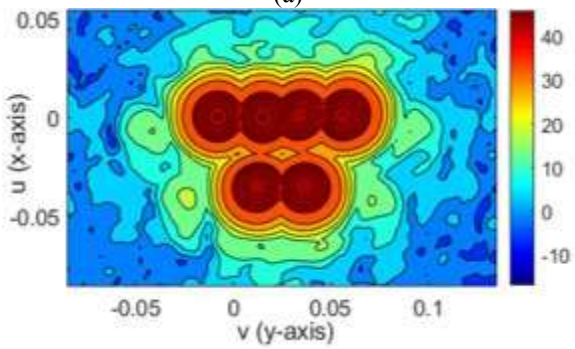

(b)

Fig. 13 Measured co-polar component of the radiation patterns provided by the reflectarray illuminated by 3 feeds at (a) 19.7 GHz and (b) 29.5 GHz.

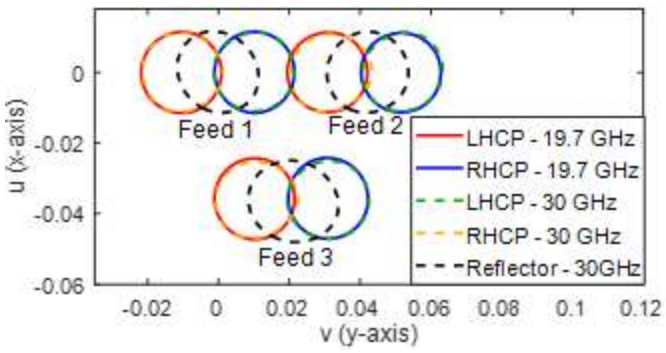

Fig. 14 Measured 40.6 dBi contours of the 6 beams generated by the reflectarray at 19.7 GHz and 30 GHz and measured 39.6 dBi contours of the 3 beams generated by the reflector at 30 GHz.

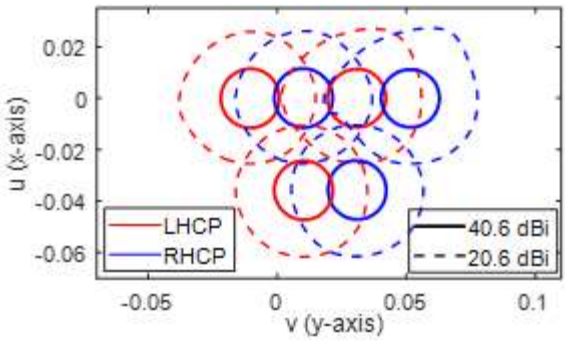

(a)

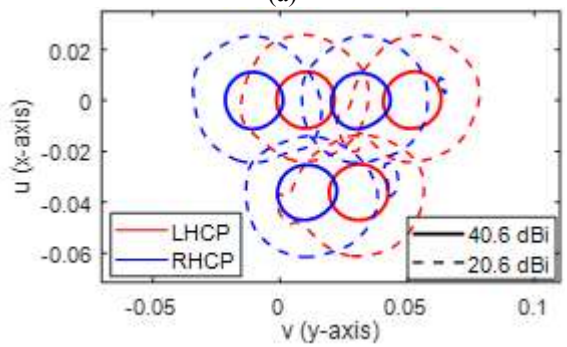

(b)

Fig. 15 Measured contours at 40.6 dBi and 20.6 dBi of the beams generated by the 3 feeds at (a) 19.7 GHz and (b) 30 GHz.

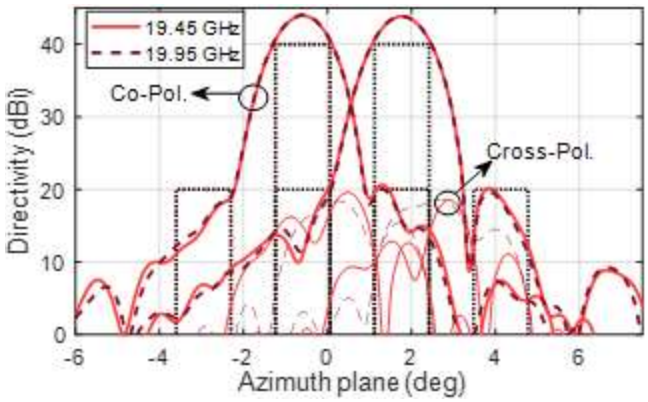

(a)

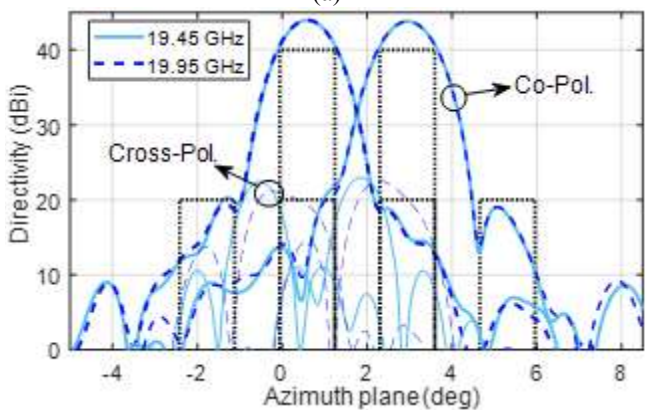

(b)

Fig. 16 Measured radiation patterns for the 'u = 0' plane at 19.45 and 19.95 GHz in (a) LHCP and (b) RHCP.

First, the performance of the manufactured reflectarray is

analyzed at the Tx band. The cuts of the radiation patterns shown in Fig. 16 and Fig. 17 are represented at 19.45 GHz and 19.95 GHz, since the higher levels of cross-polar radiation and SLL are reached at the extreme frequencies of the 500 MHz-band. Fig. 16(a) and (b) show the azimuth plane 'u = 0' for the beams generated in LHCP and RHCP, respectively, while Fig. 17 shows the azimuth plane 'u = –0.036'. As can be seen in both figures, the measured beams are close to the specification set by the masks. The six measured beams at Tx frequencies have a stable maximum directivity close to 44 dBi, while the EOC gain remains at 40.6 dBi. The single-entry C/I is higher than 20 dB for all beams except for one case, where it reaches a minimum value of 18.8 dB. Finally, the XPD shows values around 20 dB, with a minimum of 17.9 dB. Note that the simulations do not consider the polarizer included in the feed system, which has caused discrepancies in the cross-polar levels (higher in the measurements than in the simulations). The polarizer provides a nominal co-polar over cross-polar ratio of 17.6 dB in the Tx band, close to the measured XPD of the reflectarray. The inaccuracies in the assembly of the antenna structure and the reflector surface may also increase the measured cross-polar radiation.

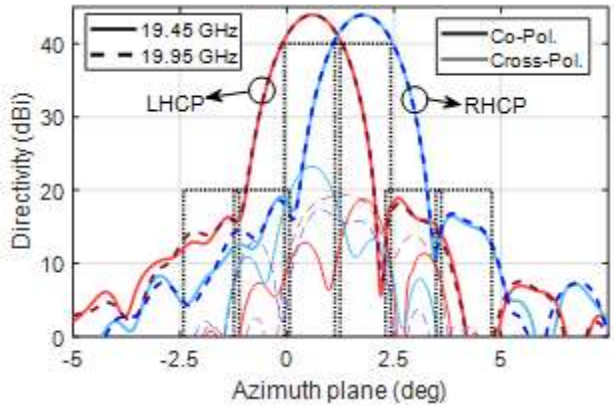

Fig. 17 Measured radiation patterns for the 'u = -0.036' plane at 19.45 and 19.95 GHz in LHCP and RHCP.

In order to compare the radiation performance of the reflectarray at the Tx band with the reference reflector antenna, Fig. 18(a) shows the measured beams at 19.7 GHz produced in dual CP by both parabolic reflectarray and reflector using the same feed position (feed 1). The measured beams associated to both antennas show similar values of maximum co- and cross-polar levels. Fig. 18(b) also shows the maximum directivity and gain of the measured beams generated by the parabolic reflectarray (D_{RA} and G_{RA} in Fig. 18(b), respectively) together with the maximum directivity and gain produced by reflector antenna (D_{ref} and G_{ref} in Fig. 18(b)), both for the case of the antenna illuminated by the central feed in LHCP for the frequencies in which the radiation patterns have been measured in the Tx band.

The difference between the maximum gain and directivity of the reference reflector is caused by the losses introduced by the feed chain, particularly by the polarizer, and by part of the spillover losses (the power radiated outside the measured angular range in the anechoic chamber), which slightly increases the directivity of the measurements. Note that the polarizer introduces larger losses at 19.2 GHz, since it is outside its operating band at Tx, and for the rest of frequencies the difference is around 0.6 dB. The difference in directivity between the reflectarray and the reflector, which reaches values lower than 0.2 dB, is produced by the losses associated to the phase errors of the reflectarray elements (not dissipative losses, but energy spread at different directions), proving the excellent performance of the reflectarray to shape the beams at the Tx band (phase errors on the reflectarray surface would produce an increase of the SLL and a reduction in the maximum directivity). Finally, the difference in measured gain between the reflectarray and the reflector comes from the total losses introduced by the reflectarray elements, reaching values lower than 0.4 dB. These losses are caused by the previously defined phase errors (0.2 dB) and the ohmic losses in the dielectrics (0.2 dB). The measured losses show an excellent performance of the reflectarray at the Tx band. The reflectarray gain also shows a small variation of around 0.4 dB within the 19.45–20.2 GHz band (inside the operating band of the polarizer). There are no differences between the maximum directivity in both CP, although the measured gains for both antennas are 0.4 dB lower in RHCP than in LHCP, which evidences a deficient performance of the polarizer.

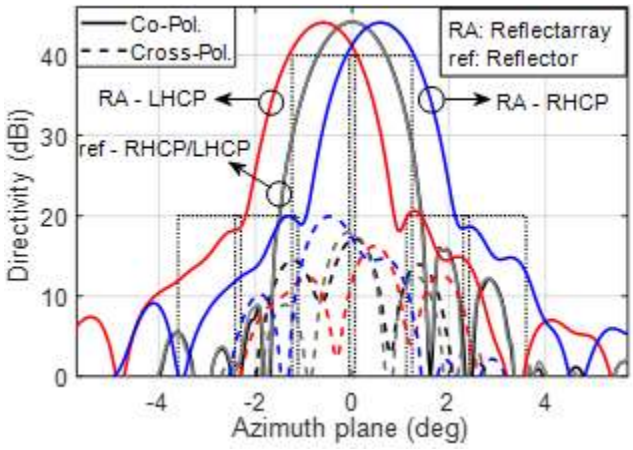

(a)

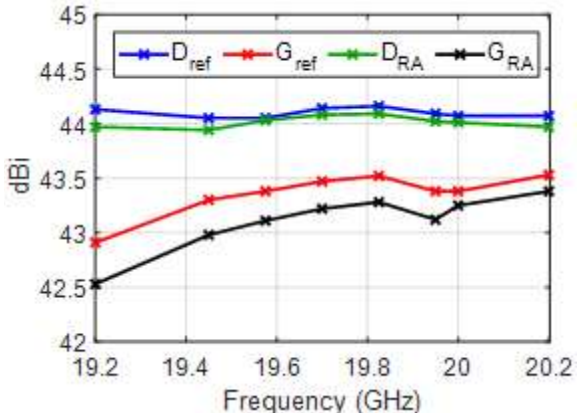

(b)

Fig. 18 (a) Measured radiation patterns at 19.7 GHz of both parabolic reflectarray and reflector for the same configuration. (b) Maximum measured directivity and gain of both reflectarray and reflector antennas in Tx band.

Now, the measurements at the Rx band are shown below (from Fig. 19 to Fig. 22). The measured radiation patterns have revealed a frequency shift in the Rx operating band: the measurements at 30 GHz show a better overall behavior in terms of cross-polar radiation and SLL than at 29.5 GHz. Fig. 19 shows the measured beams at 29.5 GHz and 30 GHz produced by the central feed. The frequency shift indicates an imprecise characterization of the dielectrics, which produces phase errors and increases the cross-polar radiation.

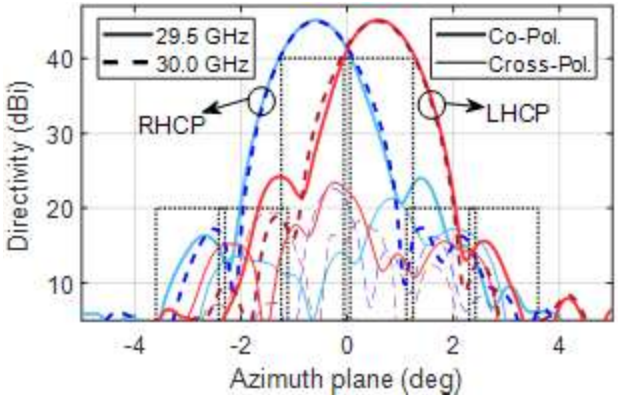

Fig. 19 Cut of the measured radiation pattern for azimuth plane at 29.5 GHz and 30 GHz for the beams generated by feed 1.

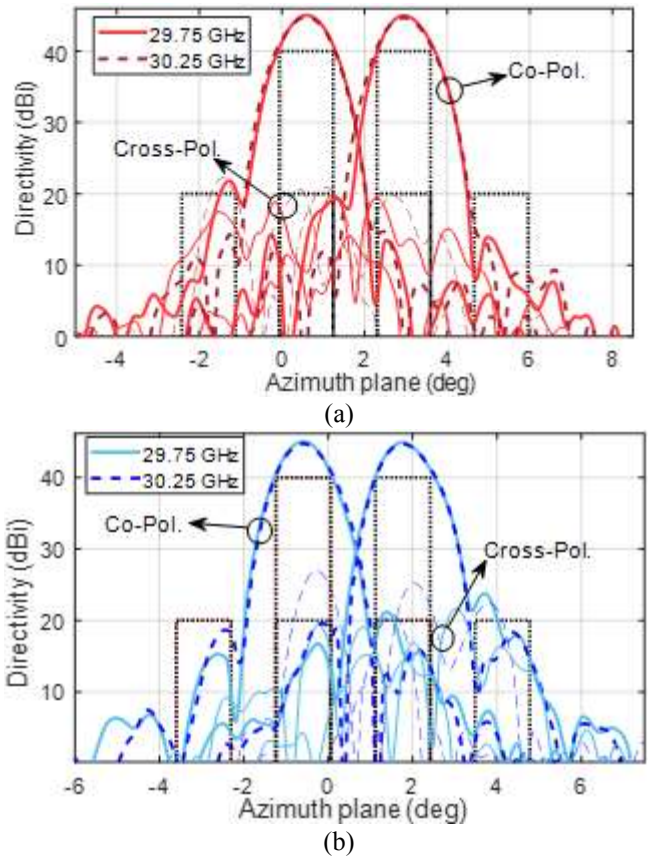

Fig. 20 Measured radiation patterns for the 'u = 0' plane at 29.75 GHz and 30.25 GHz in (a) LHCP and (b) RHCP.

According to the measurements, it has been estimated that the central frequency of the band at Rx is 30 GHz, comprising from 29.75 GHz to 30.25 GHz. As in the previous analysis at Tx, the cuts of the radiation patterns shown in Fig. 20 and Fig. 21 present measurements at the extreme frequencies of the band, in order to represent the highest levels of cross-polar radiation and SLL. Fig. 20 and Fig. 21 show the azimuth plane of the measured beams produced by the three feeds (Fig. 20 shows the cut 'u = 0' and Fig. 21 the cut 'u = – 0.036'). Both cuts of the radiation patterns present an increase of the SLL at the lower frequency (also noted in Fig. 19), and higher levels of cross-polar radiation in the RHCP measurements.

The six measured beams at Rx have a maximum directivity close to 45 dBi, 1 dB over the maximum directivity at Tx. The EOC gain (computed as the directivity where the spot diameter is 1.3º) has remained close to 40.6 dBi, the same value that was obtained for the beams in Tx. As a result, the roll-off factor at Rx reaches a level near 4.3 dB. The beams also meet the requirement of single-entry C/I (20 dB) except for one case, where it reaches a minimum value of 18.0 dB. Finally, the XPI does not comply with the required specification; the beams originated from the measurements in LHCP show a XPI that varies from 20.9 dB to 18.8 dB, while the beams originated from the measurements in RHCP present higher levels of cross-polar radiation, resulting in a XPI between 17.2 dB and 13 dB, obtained at the upper frequency (30.25 GHz). The differences in the measured cross-polar levels between the beams in RHCP and LHCP are attributed to a deficient performance of the polarizer used in the feed-chain, since the increase in cross-polar radiation caused by phase errors in the VRT implementation affects equally both polarizations. The measurements of the reference reflector also provide a similar minimum XPI of 14 dB, which confirms the unsatisfactory performance of the feed chain.

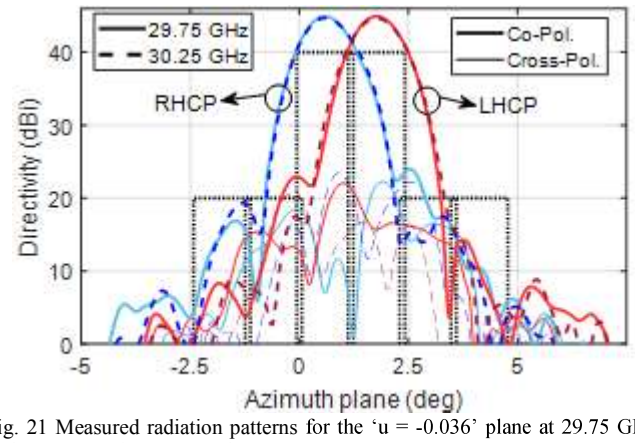

Fig. 21 Measured radiation patterns for the 'u = -0.036' plane at 29.75 GHz and 30.25 GHz in LHCP and RHCP.

The comparison between the performance of the parabolic reflectarray and the reference reflector at Rx is shown in Fig. 22. Fig. 22 (a) shows the measured beams at 30 GHz produced in dual CP by both antennas using the same feed position (feed 2). In Fig. 22(b), the measured maximum directivity and gain of the reflectarray (D_{RA} and G_{RA}) and the reflector (D_{ref} and G_{ref}) are compared for the case of the antenna illuminated by the lateral feed (feed 2) in LHCP at the Rx band.

The difference between the maximum directivity of the reflectarray and the reflector is larger than the same difference

at the Tx band because the reflectarray has been designed to introduce a phase correction that reduces the directivity around 0.5 dB at the Rx band, in order to match the roll-off requirements. In relation to the gain levels, note that the measurement system provides a relatively large uncertainty in gain (± 0.5 dB), which has caused that two measured gain values for the reflector have soared at 29.25 and 29.375 GHz (marked with red crosses in Fig. 22 (b)). The difference in gain between the reflectarray and the reflector reaches up to 0.7 dB, matching the difference between directivities, which means that the ohmic losses of the dielectric are within the uncertainty in gain of the measured system. As in the Tx frequencies, there are no differences between the measured maximum directivity of the beams in both CP, while the measured gains for both antennas are 0.6 dB lower for the beams in RHCP than in LHCP, caused by the feed-chain. Note that Fig. 22(a) shows similar cross-polar levels presents for both antennas, slightly higher for the reference reflector, caused by the feed-chain. Therefore, the performance of the parabolic reflectarray at the Rx band is highly positive.

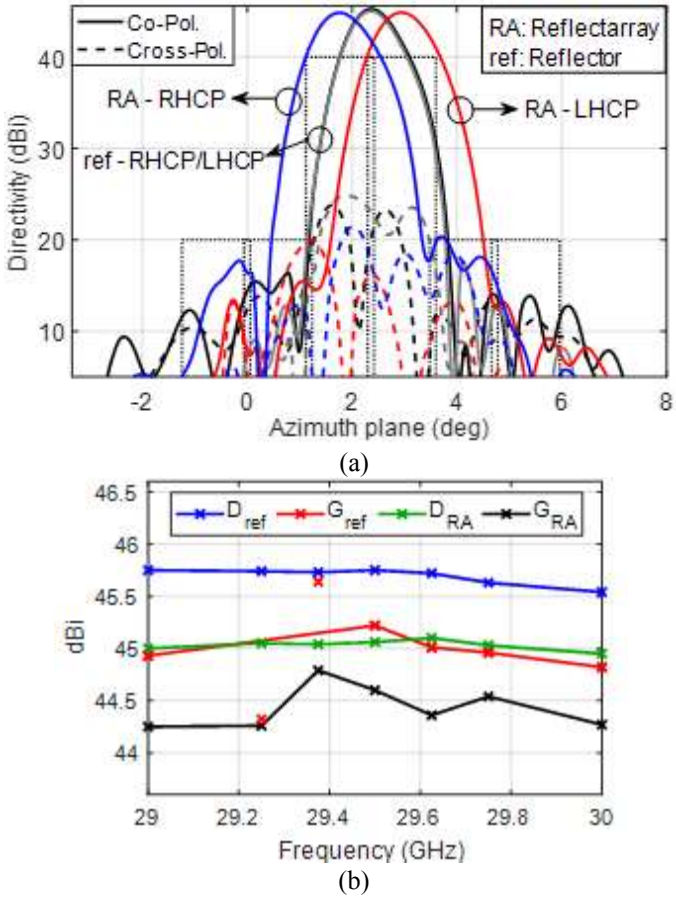

Fig. 22 (a) Measured radiation patterns at 30 GHz of both parabolic reflectarray and reflector for the same configuration. (b) Maximum measured directivity and gain of both reflectarray and reflector antennas in the Rx band.

A detailed loss budget of the parabolic reflectarray will be shown at the end of the next section, including the information provided by the measurements shown in Fig. 18 and Fig. 22 as well as simulated results to support the measured values. To summarize the measured performance of the parabolic reflectarray, Table III shows the worst measured values within the 500-MHz frequency bands (from 19.45 to 19.95 GHz for Tx, and from 29.75 to 30.25 GHz for Rx), considering both polarizations. The same EOC gain level is achieved at Tx and Rx thanks to the correction of the beam at Rx, the maximum roll-off factor is 0.1 dB higher than the specification, which falls within the measurement uncertainty, and the minimum single-entry C/I is close to the specification, with levels higher than 20 dB for most of the beams (the frequency shift in Rx has increased the SLL in that band). Finally, the minimum XPD at Tx of 17.9 dB matches the nominal XPD provided by the feed-chain, while the XPI at Rx shows a minimum value of 18.8 dB for the LHCP beams and 13 dB for the beams in RHCP. As aforementioned, the asymmetric performance of the XPI is caused by the polarizer, which also introduces 0.6 dB of additional losses in the beams in RHCP at Rx frequencies. The performance in Rx is also deteriorated due to the frequency shift. However, the measured cross-polar levels are similar to those obtained for the reference reflector, which proves the remarkable behaviour of the reflectarray.

TABLE III
MEASURED IN-BAND PERFORMANCE OF THE PARABOLIC REFLECTARRAY

Band	EOC gain (dBi)	Roll-off (dBi)	Single-Entry C/I (dB)	XPD, XPI (dB)	
				RHCP	LHCP
Tx	40.6	3.4	18.8	18.1	17.9
Rx	40.6	4.4	18	13	18.8

B. *Comparison between Measurements and Simulations*

The measurements at Tx show a quite good agreement with the simulated results shown in Section V, with small differences in the maximum levels of the cross-polar radiation, as it was expected, since the cross-polar produced by the feed assembly was not included in the simulations. However, the measurements at Rx present a frequency shift of 0.5 GHz and higher SLL and cross-polar levels than the simulations.

The dimensions of the printed elements were checked after the fabrication, showing an averaged error of -10 μm in the dimensions of both arcs and dipoles, plus a random error of ±5 μm. This error was included in the simulations, showing a negligible effect at Tx but increasing the SLL at Rx. In order to determine the cause of the shift in frequency at Rx, the electrical properties of the substrate IsoClad 933 has been characterized by some samples formed by two reflectarray cells printed on the same substrate used for the reflectarray. The samples have been measured using the waveguide simulator technique (WGS) to test the performance of the reflectarray cell in a periodic environment [32]. The results showed that the initial permittivity considered in the simulations should be changed to $\varepsilon_r = 2.4$.

Note also that the previous simulations showed gain levels, while the measured radiation cuts represent directivity to reduce the uncertainty of the measurement system. To compare both measurements and simulations in directivity, the dissipative losses associated to the substrates have been suppressed in the simulation process. In this way, the

maximum level of the simulated directivity has increased 0.2 dB at 19.7 GHz and 0.4 dB at 29.5 GHz. The last effect to be excluded in the simulations is the radiated power outside the angular range of the measurements, increasing the directivity 0.3 dB at 19.7 GHz and 0.8 dB at 29.5 GHz.

Fig. 23 shows the measured and simulated radiation patterns of the beams generated by the central feed in LHCP at 19.7 GHz and in RHCP at 29.5 GHz, considering the corrected simulations. As can be seen, the measurements and the corrected simulations show an excellent agreement, with a difference between measured and simulated maximum levels of directivity lower than 0.2 dB, which is the uncertainty of the measurements. As aforementioned, the discrepancies in the cross-polar component are caused by the effect of the polarizer in the feed chain, not considered in the simulations.

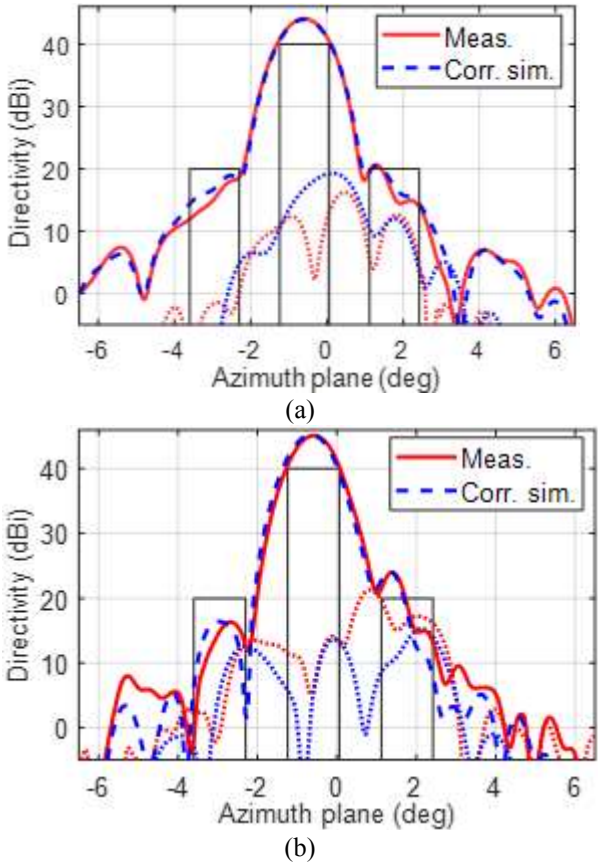

Fig. 23 Measured and simulated radiation patterns of the beam generated by feed 1 in (a) LHCP at 19.7 GHz and (b) RHCP at 29.5 GHz.

A detailed antenna loss budget is shown in Table IV considering the measured directivity and gain of the reference reflector and the parabolic reflectarray (D_{ref}, G_{ref}, D_{RA}, G_{RA}) shown in Fig. 18 and Fig. 22, and the simulated values provided in this section. The loss budget is divided into three main components. The first component, related to the illumination losses, is the difference between the measured directivity of the reference reflector (D_{ref}) and the theorical directivity of a reflector antenna $D_{theo} = 10\log_{10}((\pi \cdot D/\lambda)^2)$. In contrast to D_{theo}, D_{ref} includes the losses produced by the taper and spillover efficiencies, and by the shift of the phase center of the feed-horn (only at Rx frequencies) as well as the increment ξ due to the radiated power lost outside the measured angular range in the anechoic chamber. The taper and spillover efficiencies (67% and 92%, respectively at Tx, and 48% and 98%, at Rx) have been estimated from the simulated taper illumination in the prototype. The second component, given by the difference between the measured directivity and gain of the reference reflector ($D_{ref} - G_{ref}$), is composed of the increment ξ and the losses associated to the feed chain. The last component ($G_{ref} - G_{RA}$) represents the losses introduced by the reflectarray elements, which can be divided into the losses associated to phase errors ($D_{ref} - D_{RA}$), and the ohmic losses associated to the substrates. In this way, each component of the table is divided in its main factors, estimated by measurements or simulations, which support each other: the sum of the factors associated to the illumination losses matches the total illumination losses within the uncertainty of the measurements, as well as the resulting feed losses and the nominal insertion losses of the polarizer, or the dielectric losses obtained by measurements and simulations. Table IV proves an excellent performance of the prototype, with a total level of losses introduced by the reflectarray elements similar to that of single-layer reflectarrays [20].

TABLE IV
ANTENNA LOSS BUDGET

FIGURE OF MERIT		Tx	Rx
Taper illumination		−12 dB	−18 dB
Illumination losses ($D_{theo} - D_{ref}$)	Total losses	1.6 dB	3.2 dB
	Taper	1.7 dB	3.2 dB
	Spillover	0.35 dB	0.09 dB
	Shift of phase center	0 dB	0.5 dB
	Power lost (ξ)	−0.3 dB	−0.8 dB
Feed losses and radiated power lost ($D_{ref} - G_{ref}$)	Total losses	0.6 dB	0.8 dB
	Power lost (ξ)	0.3 dB	0.8 dB
	Feed losses ($D_{ref} - G_{ref}$) − ξ	0.3 dB (0.45 dB nominal)	0 dB (0.35 dB nominal)
Reflectarray losses ($G_{ref} - G_{RA}$)	Total losses	0.4 dB	0.7 dB
	Phase errors ($D_{ref} - D_{RA}$)	0.2 dB	0.8 dB
	Dielectric Losses ($G_{ref} - G_{RA}$) − ($D_{ref} - D_{RA}$)	0.2 dB (0.2 dB in sims.)	0 dB (0.4 dB in sims.)

VII. CONCLUSION

For the first time, a 0.9 m parabolic multilayer reflectarray has been designed, manufactured and measured to generate two spaced beams per feed in orthogonal CP with improved cross-polarization in the Tx and Rx frequencies used in Ka-band satellites. The parabolic reflectarray also demonstrates for the first time that the two beams per feed are in orthogonal CP at Tx and Rx frequencies, while maintaining the cross-polar radiation as moderate as that obtained with an equivalent reflector in the entire frequency bands. The measured results show an excellent behavior with a high degree of compliance with the required specifications. The corrected simulations also show a

great agreement with the measurements in both frequency bands, validating the design technique, as well as the simulation homemade codes.

This concept can be suitable for multispot satellites in Ka-band, since a single parabolic reflectarray can generate half of the required multi-spot coverage (two colors), making it possible to halve the number of antennas and feed-chains required on board the HTS, from four reflectors antennas to two parabolic reflectarray using a SFB configuration.

ACKNOWLEDGMENT

The authors would like to thank Acom Sistemas for developing the manufacturing process of the antenna system and Trackwise for the photo-etching process of the manufactured reflectarray. The authors would also like to thank Anteral for providing the feed-horn and to Prof. Jorge Teniente from Public University of Navarra, for his valuable help in the feed characterization using spherical mode expansion.

REFERENCES

[1] H. Fenech, S. Amos, A. Tomatis, and V. Soumpholphakdy, "High throughput satellite systems: An analytical approach," *IEEE Trans. Aerosp. Electron. Syst*., vol. 51, no. 1, pp. 192-202, Jan. 2015.

[2] M. Schneider, C. Hartwanger and H. Wolf, "Antennas for multiple spot beams satellites", *CEAS Space Journal*, Vol. 2, pp. 59-66, Dec. 2011.

[3] G. Toso, C. Mangenot and P. Angeletti, "Recent advances on space multibeam antennas based on a single aperture," *7th European Conference on Antennas and Propagation (EuCAP 2013*), Gothenburg, 2013, pp. 454-458.

[4] O. M. Bucci, T. Isernia, S. Perna and D. Pinchera, "Isophoric sparse arrays ensuring global coverage in satellite communications", *IEEE Trans. Antennas Propag.*, vol. 62, no. 4, pp. 1607-1618, Apr. 2014.

[5] P. Bosshard et al., "Thales Alenia Space HTS/V-HTS Multiple Beam Antennas Sub-systems on the Right Track", *10th European Conference on Antennas and Propagation (EuCAP 2016)*, Davos, Switzerland, Apr. 2016, pp.1-5

[6] E. Martinez-de-Rioja, D. Martinez-de-Rioja, J. A. Encinar, A. Pino, B. Gonzalez-Valdes, Y. Rodriguez-Vaqueiro, M. Arias, and G. Toso, "Advanced Multibeam Antenna Configurations Based on Reflectarrays: Providing Multispot Coverage With A Smaller Number of Apertures for Satellite Communications in the K and Ka Bands", *IEEE Antennas Propag. Mag.*, Vol. 61, No. 5, pp. 77 – 86, Oct. 2019.

[7] J. A. Encinar, L. Datashvili, J. Agustín Zornoza, M. Arrebola, M. Sierra–Castañer, J. L. Besada, H. Baier, H. Legay "Dual–Polarization Dual–Coverage Reflectarray for Space Applications", *IEEE Trans. Antennas Propag.,* 54(10), 2006, 2827–2837.

[8] S. R. Rengarajan, "Reflectarrays of rectangular microstrip patches for dual-polarization dual-beam radar interferometers", *Progress In Electromagnetics Research*, Vol. 133, pp. 1–15, 2013.

[9] S. Mener, R. Gillard, R. Sauleau, A. Bellion, and P. Potier, "Dual-circularly polarized reflectarray with independent control of polarizations," *IEEE Trans. Antennas Propag*., vol. 63, no. 4, pp. 1877–1881, April 2015.

[10] M. Hosseini and S. V. Hum, "A dual-CP reflectarray unit cell for realizing independently controlled beams for space applications", in *Proc. 11th European Conference Antennas Propag. (EuCAP 2017)*, Paris, France, April 2017, pp. 66-70.

[11] C. S. Geaney, M. Hosseini and S. V. Hum, "Reflectarray Antennas for Independent Dual Linear and Circular Polarization Control," in *IEEE Trans. Antennas Propag.*, vol. 67, no. 9, pp. 5908-5918, Sept. 2019.

[12] J. Huang and R. J. Pogorzelski, "A Ka-band microstrip reflectarray with elements having variable rotation angles," *IEEE Trans. Antennas Propag.*, vol. 46, no. 5, pp. 650–656, 1998.

[13] T. Smith, U. Gothelf, O. S. Kim, and O. Breinbjerg, "Design, manufacturing, and testing of a 20/30-GHz dual-band circularly polarized reflectarray antenna," *IEEE Antennas Wireless Propag. Lett*., vol. 12, pp. 1480–1483, 2013.

[14] M. Zhou and S. B. Sørensen, "Multi-spot beam reflectarrays for satellite telecommunication applications in Ka-band", *Proc. 10th European Conference Antennas Propag. (EuCAP 2016)*, Davos, 2016, pp.1-5.

[15] A. Somolinos R. Florencio, I. González, J. A. Encinar and F. Cátedra, "Experimental Validation of Generating Two Spaced Beams with Reflectarrays by VRT", *IEEE Trans. Antennas Propag.*, vol. 67, no. 6, pp. 4263 – 4268, June 2019.

[16] R. Florencio, J. A. Encinar, R. R. Boix, M. Barba and G. Toso, "Flat Reflectarray that Generates Adjacent Beams by Discriminating in Dual Circular Polarization", *IEEE Trans. Antennas Propag*., vol. 67, no. 6, pp. 3733 – 3742, June 2019.

[17] D. Martinez-de-Rioja, R. Florencio, J. A. Encinar, E. Carrasco, Rafael R. Boix, "Dual Frequency Reflectarray Cell to Provide Opposite Phase-Shift in Dual Circular Polarization with Application in Multibeam Satellite Antennas", *IEEE Antennas Wireless Propag. Lett*., vol. 18, no. 8, pp. 1591 – 1595, Aug. 2019.

[18] D. Martinez-de-Rioja, R. Florencio, E. Martinez-de-Rioja, M. Arrebola, J. A. Encinar, Rafael R. Boix, "Dual-Band Reflectarray to Generate Two Spaced Beams in Orthogonal Circular Polarization by Variable Rotation Technique", *IEEE Trans. Antennas Propag*., vol. 68, no 6, pp. 4617-4626, June 2020.

[19] M. Zhou, S. B. Sørensen, N. Vesterdal, M. F. Palvig, Y. Brand, S. Maltais, J. Bellermore, G. Toso, "Design of Dual-Band Dual-Polarized Reflectarray for Future Multiple Spot Beam Applications in Ka-band", *13th European Conference Antennas Propag. (EuCAP 2019)*, Krakow, 2019, pp.1-5.

[20] M. Zhou, S. B. Sørensen, Y. Brand, G. Toso, "Doubly Curved Reflectarray for Dual-Band Multiple Spot Beam Communication Satellites", *IEEE Trans. Antennas Propag*, vol. 68, no. 3, pp. 2087-2096, March 2020.

[21] H. Fenech, S.Amos, A. Tomatis, V. Soumpholphakdy, "KA-SAT and Future HTS Systems" *IEEE 14th International Vacuum Electronics Conference (IVEC 2013)*, Paris, France, May 2013.

[22] R. Florencio, R. R. Boix, E. Carrasco, J.A. Encinar, V. Losada. (2013), "Efficient numerical tool for the analysis and design of reflectarrays based on cells with three parallel dipoles". *Microw. Opt. Technol. Lett.*, Vol. 55, no. 6, pp. 1212-1216, June 2013.

[23] R. Florencio, R. R. Boix and J. A. Encinar, "Efficient Spectral Domain MoM for the Design of Circularly Polarized Reflectarray Antennas Made of Split Rings," in *IEEE Trans. Antennas Propag.*, vol. 67, no. 3, pp. 1760-1771, March 2019.

[24] Rogers IsoClad 933 laminates. [Online]. Available: https://rogerscorp.com/advanced-connectivity-solutions/isoclad-series-laminates/isoclad-933-laminates, Accessed on April 29, 2020.

[25] J. D. Vacchione, R. C. Kruid, A. Prata, L. R. Amaro and A. P. Mittskus, "Telecommunications antennas for the Juno Mission to Jupiter," *2012 IEEE Aerospace Conference*, Big Sky, MT, 2012, pp. 1-16.

[26] Anteral. [Online]. Available: https://anteral.com Accessed on Jan. 04, 2020.

[27] General Dynamics. [Online]. Available: https://www.gd.com/ Accessed on Jan. 29, 2020.

[28] Y. Rahmat-Samii, "A comparison between GO/aperture-field and physical-optics methods of offset reflectors," in *IEEE Trans. Antennas Propag.*, vol. 32, no. 3, pp. 301-306, March 1984. doi: 10.1109/TAP.1984.1143300.

[29] Trackwise. [Online]. Available: https://www.trackwise.co.uk/ Accessed on Jan. 09, 2020.

[30] Acom Sistemas. [Online]. Available: http://acomsistemas.es/ Accessed on Jan. 04, 2020.

[31] R. Caballero, C. Palacios, J. A. Encinar, "Mars Express and Venus Express High Gain Antennas", *27th ESA Antenna workshop on Innovative Periodic Antennas*, 9-11 March 2004, Santiago de Compostela, Spain, pp. 83-89.

[32] P. W. Hannan, M. A. Balfour, "Simulation of phased array antennas in waveguides", *IEEE Trans. Antennas Propag., Vol. 13, pp. 342-353*, May 1965.

Daniel Martinez-de-Rioja (S'18) was born in Madrid, Spain. He received the B.Sc. and M.Sc. degrees in telecommunication engineering from the Universidad Politécnica de Madrid (UPM), Madrid, in 2016 and 2018, respectively.

Since 2016, he has been a Student Research Assistant with the Applied Electromagnetics Group, UPM. His current research interests include the design of dual frequency, dual-polarization, and multibeam reflectarray antennas for satellite applications in Ka-bands.

Mr. Martinez-de-Rioja is a recipient of a pre-doctoral fellowship from the Spanish Ministry of Economy and Competitiveness.

Eduardo Martinez-de-Rioja (S'15–M'18) was born in Madrid, Spain. He received the Telecommunication Engineer and Ph.D. degrees from the Universidad Politécnica de Madrid (UPM), Madrid, in 2014 and 2018, respectively.

From 2015 to 2019, he was with the Applied Electromagnetics Group at UPM, as a Research Assistant. In 2016, he joined the Electrical and Computer Engineering Department, University of Toronto, Toronto, Canada, as a Visiting Ph.D. Student. Since 2019, he is an Assistant Professor at the Department of Signal Theory and Communications and Telematic Systems and Computing, Universidad Rey Juan Carlos, Madrid, Spain. His research interests include the design of dual-frequency, dual-polarization and multibeam reflectarray antennas for satellite applications in Ku and Ka bands.

Dr. Martinez-de-Rioja was a recipient of the 2019 National Awards of the Spanish Official College of Telecommunication Engineers to the Best Ph.D. Thesis in the category of Government Satellite Services.

Yolanda Rodriguez-Vaqueiro received the B.S. and M.S. degrees in electrical engineering from the University of Vigo, Vigo, Spain, in December 2009, and the Ph.D. degree in electrical engineering from Northeastern University, Boston, MA, USA, in May 2015, with thesis on "Compressive Sensing for Electromagnetic Imaging Using a Nesterov-Based Algorithm.".

She was a Junior Researcher with the University of Vigo, where she is currently a Postdoctoral Researcher affiliated with AtlantTIC Research Center. In 2011, she received a Research Assistant grant from the Awareness and Localization of Explosive Related Threats (ALERT) Center of Excellence, Northeastern University.

Dr. Rodriguez-Vaqueiro was recognized with the "Research-Impact Award" by the Electrical and Computer Engineering Department, Northeastern University, for the Ph.D. studies. During the course of her career, she was the recipient of several awards: "Best Paper Award" in the 2012 IEEE Homeland Security Conference, "Honorable Mention in the Student Paper Competition" in the 2013 IEEE IEEE Antennas and Propagation Society International Symposium, "Best Paper Award" in the 2014 European Conference on Antennas and Propagation, and "Burke/Yannas Award" for the most original research study in the field of bioengineering in the 2015 American Burn Association Meeting. In 2018, she was awarded with a "Juan de la Cierva" grant by the Spanish Ministry of Education.

José A. Encinar (S'81–M'86–SM'09–F'10) was born in Madrid, Spain. He received the Electrical Engineering degree and the Ph.D. degree from the Universidad Politécnica de Madrid (UPM), Madrid, in 1979 and 1985, respectively.

He was with the Laboratory of Electromagnetics and Acoustics, École Polytechnique Fédérale de Lausanne (EPFL), Lausanne, Switzerland, in 1996, and with the Institute of Electronics, Communication and Information Technology (ECIT), Queen's University Belfast, Belfast, U.K., in 2006 and 2011, as a Visiting Professor. Since 1980, he has been with the Applied Electromagnetism and Microwaves Group, UPM, where he was a Teaching and Research Assistant from 1980 to 1982, an Assistant Professor from 1983 to 1986, and an Associate Professor from 1986 to 1991. Since 1987, he has been a Post-Doctoral Fellow of the NATO Science Program with Polytechnic University, New York City, NY, USA. Since 1991, he has been a Professor with the Electromagnetism and Circuit Theory Department, UPM. He has authored or co-authored over 100 and 50 journal and conference papers, and he holds five patents on array and reflectarray antennas. His current research interests include numerical techniques for the analysis of multilayered periodic structures, design of frequency selective surfaces, printed arrays, and reflectarrays.

Dr. Encinar is a member of the Technical Program Committee of several International Conferences (European Conference on Antennas and Propagation, ESA Antenna Workshops, and Loughborough Antennas and Propagation Conference). He was a co-recipient of the 2005 H. A. Wheeler Applications Prize Paper Award and the 2007 S. A. Schelkuno Transactions Prize Paper Award given by the IEEE Antennas and Propagation Society.

Antonio Pino (S'87–M'89–SM'05) was born in Madrid, Spain, in 1962. He received the M.S. and Ph.D. degrees in telecommunications engineering from the Polytechnic University of Madrid (UPM), Madrid, in 1985 and 1989, respectively.

From 1985 to 1989, he was with the Radiation Group, UPM, as a Research Assistant. He joined the Department of Technologies of Communications, University of Vigo, Vigo,

Spain, as an Associate Professor in 1989, and became a Full Professor in 1994. During 1993, he was a Visiting Researcher with the Center for Electromagnetics Research, Northeastern University, Boston, MA, USA. From 2006 to 2010, he was the Vice-Rector with Academic Organization and Faculty, University of Vigo, and since 2014, has been the Director with the International Doctoral School, University of Vigo. He has authored more than 100 technical papers in journal and conferences and has been an Advisor of 14 Ph.D. thesis. His research interests include reflectarray and shaped reflector antennas for communication and radar applications, high-frequency backscattering, computational electromagnetics, and terahertz technology.

Marcos Arias was born in Vigo, Spain, on June 1, 1968. He received the Telecommunications Engineer degree and the Ph.D. degree in telecommunication engineering from the University of Vigo, Vigo, in 1991 and 1997, respectively.

He has been an Associate Professor since 1998 and has been with the Department of Signal Theory and Communications teaching radiocommunications, University of Vigo, since 1992. He has worked in projects related with antennas for satellite and radioastronomy, communication systems such Digital Video Broadcasting-Terrestrial, Local Multipoint Distribution System, and Universal Mobile Telecommunications System, and system engineering.

Giovanni Toso (S'93–M'00–SM'07) received the Laurea Degree (cum laude), the Ph.D. and the Post Doctoral Fellowship from the University of Florence, Italy, in 1992, 1995 and 1999. In 1996 he was visiting scientist at the Laboratoire d'Optique Electromagnétique, Marseille (France). In 1999 he was a visiting scientist at the University of California (UCLA) in Los Angeles, he received a scholarship from Alenia Spazio (Rome, Italy) and he has been appointed researcher in a Radio Astronomy Observatory of the Italian National Council of Researches (CNR). Since 2000 he is with the Antenna and Submillimeter Waves Section of the European Space Agency, ESA ESTEC, Noordwijk, The Netherlands. He has been initiating and contributing to several R&D activities on satellite antennas based on arrays, reflectarrays, lenses and reflectors.

G. Toso has been coauthoring the best paper at the 30th ESA Antenna Workshop and the most innovative paper at the 30th and 36th ESA Antenna Workshops. In 2009 he has been coeditor of the Special Issue on Active Antennas for Satellite Applications in the International Journal of Antennas and Propagation. In 2014 he has been guest editor, together with Dr. R. Mailloux, of the Special Issue on "Innovative Phased array antennas based on non-regular lattices and overlapped subarrays" published in the IEEE Transactions on Antennas and Propagation and, for the same society, has been an Associate Editor (2013-2016). Since 2010, together with Dr. P. Angeletti, he has been instructing short courses on Multibeam Antennas and Beamforming Networks during international conferences (IEEE APS, IEEE IMS, IEEE IWCS, EUCAP, EuMW) that have been attended by more than 600 participants. In 2018, G. Toso received with Prof. A. Skrivervik the Best Teacher Award of the European School of Antennas (ESoA) out of 101 teachers.